



Synthesis and preliminary study of pure and Zr-doped YMnO_3 compounds as Solid Oxide Fuel Cells electrode



Zulma Liliana Moreno Botello ^{a, b}, Alberto Caneiro ^b, Pascal Roussel ^c, Gilles Gauthier ^{a, *}

^a Universidad Industrial de Santander, Grupo INTERFASE, Ciudad Universitaria, Calle 9, Carrera 27, Bucaramanga (Santander), Colombia

^b Centro Atómico Bariloche, Comisión Nacional de Energía Atómica, Av. Bustillo 9500, 8400, S. C. de Bariloche, Argentina

^c Université Lille Nord de France, Unité de Catalyse et de Chimie du Solide (UCCS – CNRS UMR8181), ENSCL–USTL, BP90108, 59652 Villeneuve d'Ascq, France

ARTICLE INFO

Article history:

Received 28 May 2016

Received in revised form

6 August 2016

Accepted 14 August 2016

Available online 17 August 2016

Keywords:

Solid Oxide Fuel Cells

Electrode

Yttrium manganite

Reducibility

Reactivity

ABSTRACT

The $\text{Y}_{1-x}\text{Zr}_x\text{MnO}_3$ series ($0 \leq x \leq 0.30$) has been studied to be used as possible SOFC electrode material. These compounds adopt a layered structure of hexagonal symmetry in which the manganese cations are located in trigonal bi-pyramidal coordination of oxygen atoms, different from that of the classical perovskite. The synthesis of the materials has been carried out by solid state reaction and X-ray diffraction technique reveals that pure phases can be obtained until $x=0.10$. For $x \geq 0.10$, an additional YSZ phase is formed, similar to the SOFC electrolyte material. HT-XRD technique and thermogravimetric analysis of pure or Zr-doped YMnO_3 indicate that, in diluted dry H_2 for $T > 600^\circ\text{C}$, these compounds are unstable, what precludes their use as anode material. On the other hand, reactivity studies at high temperature ($T = 1300^\circ\text{C}$) between $\text{Y}_{1-x}\text{Zr}_x\text{MnO}_3$ ($x = 0, 0.05$ and 0.1) and 8YSZ show a chemical compatibility in which the formation of an electrically insulating phase does not take place, but a crossed diffusion of $\text{Y}^{3+}/\text{Mn}^{3+}$ and Zr^{4+} at the interface between both materials. Thermomechanical compatibility in air between YSZ and $\text{Y}_{1-x}\text{Zr}_x\text{MnO}_3$ is also demonstrated from RT to 850°C .

© 2016 Elsevier B.V. All rights reserved.

1. Introduction

Given the increasing of different environmental problems and the possibility of a global energetic crisis, finding ways that are more efficient for energy generation is of major importance for generations to come. The Solid Oxide Fuel Cells (SOFC) are considered as one of the most viable solutions for the future, as it can operate either with hydrogen, the non-polluting fuel by excellence, or with any organic fuel, fossil or synthetic, with a relatively higher efficiency of conversion than other more classical technologies [1–3]. Unfortunately, the state-of-the-art materials used to fabricate SOFCs are already not giving complete satisfaction in terms of efficiency and durability, especially because of chemical reactivity at the interfaces during cell preparation or *in operando*; this is especially the case at the cathode side, the main degradation occurring from the reactivity between the electrode and both electrolyte or interconnect [4,5]. Moreover, the Ni/YSZ cermet (YSZ = yttria-doped zirconia) currently employed at the anodic side

presents many problems during redox cycling and Ni coarsening in temperature, in addition to issues related to complex organic fuel utilization (coking, poisoning with sulfur, ...) [6].

While most of the research done in the area is focused on perovskite oxides, this study goes aboard on the study of manganites of a different structure type. Indeed, REMnO_3 oxides can crystallize into two distinct ways depending on the size of the rare earth (RE) cation with respect to Mn: when the RE ionic radius is large (La–Tb) the structure adopts the perovskite arrangement, but if it is small (Dy–Lu, Y, Sc), the material becomes layer-type [7,8]. In particular, YMnO_3 crystallizes in the hexagonal $P6_3cm$ space group. As depicted in Fig. 1, the structure is built of $[\text{MnO}_5]$ trigonal bi-pyramids (instead of octahedra in perovskites) linked by their three equatorial vertices to form layers. The latter are in turn separated by layers of Y^{3+} cations in 8-fold bi-capped trigonal antiprisms of oxygen (instead of 12-fold for the RE site in perovskites), the $[\text{YO}_8]$ polyhedra being linked to the apical oxygen ions of the bi-pyramids [7]. The stability of the hexagonal layered structure of REMnO_3 stoichiometry with respect to the perovskite is mainly due to the low value of the Goldschmidt tolerance factor ($t < 0.855$) because of a small RE cation [9,10]. Indeed, YMnO_3 can be prepared in both structural types, but the hexagonal layered compound (h- YMnO_3) is

* Corresponding author.

E-mail address: gilgau@uis.edu.co (G. Gauthier).

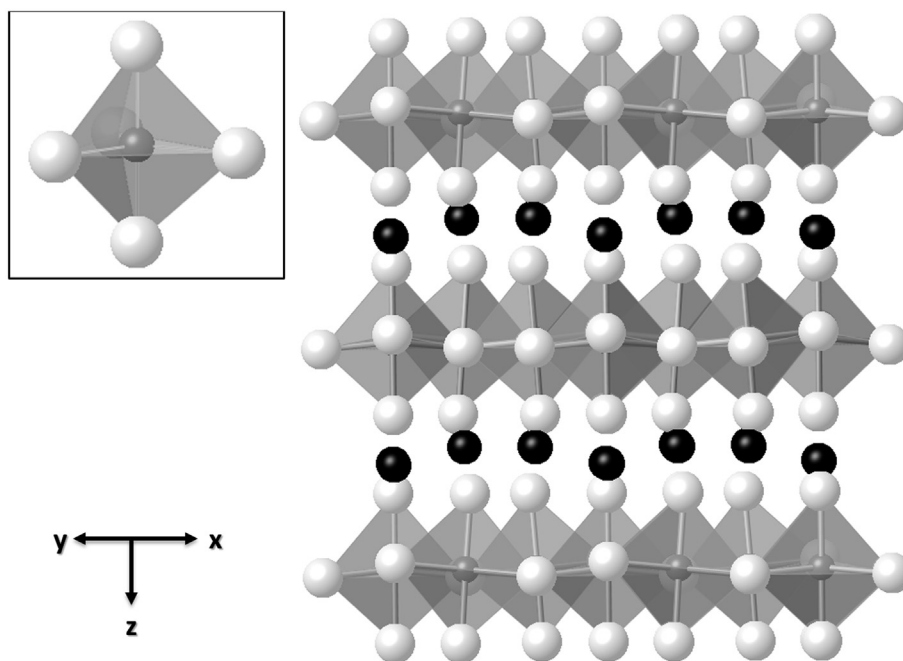


Fig. 1. Representation of hexagonal YMnO_3 structure. Buckled layers of Y atoms (black) in 8-fold coordination of O atoms (light gray) separate the $[\text{MnO}_5]$ trigonal bi-pyramids (dark gray) layers in which each polyhedron is linked to three other by their equatorial vertices.

more stable in usual temperature and pressure conditions. As an example, h-YMnO_3 can be synthesized by solid state method in air at 1200°C under ambient pressure [8] whereas the orthorhombic perovskite structure is stabilized by either low-temperature [11], high-pressure synthesis [12], or even epitaxial thin film growth [13].

According to literature, YMnO_3 can be doped by aliovalent cations, as in the case in which Y^{3+} cations are replaced by Zr^{4+} , forming a hexagonal solid solution for $x < 0.3$ compositions [14–18]. According to Van Aken *et al.* [14], the doping the structure with Zr^{4+} conduces to $\text{Mn}^{2+}/\text{Mn}^{3+}$ mixed valence with a decrease of lattice parameters. Nevertheless, another work indicates that single phased materials cannot be obtained for concentrations higher than $x = 0.1$ in the $\text{Y}_{1-x}\text{Zr}_x\text{MnO}_3$ series; beyond such value, precipitation of ZrO_2 -type material occurs [15]. Some authors also indicate the possibility of substituting Ca^{2+} or Sr^{2+} for Y^{3+} and forming the $\text{Y}_{1-x}\text{A}_x\text{MnO}_3$ ($\text{A} = \text{Ca}, \text{Sr}$) solid solution hexagonal structure for $x < 0.22$ [16,17]. In this case, acceptor doping induces a $\text{Mn}^{3+}/\text{Mn}^{4+}$ mixed valence that provides p-type carriers and higher conductivity level respect to that of Zr-doping [14]. However, other studies claim that Ca-doping is not possible in YMnO_3 and such substitution always gives a mixture including an orthorhombic perovskite phase [17]. Moreover, Sr-doping in YMnO_3 would induce, as in the case of Sr-doped LaMnO_3 (LSM), a strong chemical reactivity with the YSZ electrolyte [18]; such reactivity would be probably the case for Ca-doping too, which is not acceptable for the application.

Finally, different results describe the non-stoichiometry possibilities in REMnO_3 hexagonal manganites; according to T. Atsumi *et al.* [19], $\text{YMnO}_{3-\delta}$ can be oxygen deficient until the maximum value $\delta \sim 0.04$, confirmed more recently by the parent composition $\text{DyMnO}_{3-\delta}$ by Remsen *et al.* [20]. The latter work also describe that the RMnO_3 family displays oxygen excess considerable oxygen positive non-stoichiometry, until $\delta \sim 0.18$ for $\text{R} = \text{Dy}$ in air, which gives insight of some aptitude for donor doping. On the other hand, the soft chemistry reduction of YMnO_3 using a calcium hydride

probe to be stable until $\text{YMnO}_{2.80}$ and interesting structural features give hope for a possible Mixed Ionic Electronic Conducting (MIEC) behaviour *i.e.* the possibility to use such manganites as SOFC electrode materials: (i) the reduced compounds present oxygen vacancies localized in the equatorial planes with an increasing disorder in the tilting that could be associated to higher oxygen (or oxygen vacancy) mobility; (ii) the reduction induces a structural change to the more symmetrical space group $P6_3/mmc$ for which the $[\text{MnO}_5]$ bi-pyramids are not yet cooperatively tilted and the Y planes not buckled [21].

The aim of this preliminary study is to clarify the possibility of doping Zr for Y in YMnO_3 but also to evaluate the possible use of such pure or donor-doped materials as anode and/or cathode component in Solid Oxide Fuel Cells, based on tests of chemical and thermomechanical compatibility with SOFC electrolyte YSZ and reducibility in diluted hydrogen atmosphere.

2. Materials and methods

Non-doped YMnO_3 powder was prepared by solid-state reaction using Y_2O_3 (Alfa Aesar, 99.9%, previously treated at 1000°C for 3 h) and MnO_2 (Alfa Aesar, 99.9%, dried at 150°C for 3 h) as precursors. Stoichiometric amounts of the corresponding powders were thoroughly weighed, mixed and ground together before being pressed into pellets that were placed on alumina foils using sacrificial powder bed. The heat treatment were performed at 1400°C during 12 h in air using heating and cooling rates of 4°C min^{-1} . For the doped $\text{Y}_{1-x}\text{Zr}_x\text{MnO}_3$ samples ($x = 0.05, 0.1, 0.15, 0.2$ and 0.3 , thereafter referred as YZM), Zr (IV) isopropoxide (Alfa Aesar, 99.9%), previously treated at 1000°C for 3 h was used as zirconium source. In this case, the pressed pellets were placed on platinum foils due to greater reactivity with alumina, then treated in air at 1400°C , 1450°C and finally 1500°C , each time for 12 h, with intermediate grinding steps.

Phase analysis was performed after synthesis by X-ray diffraction at room temperature using a BRUKER D8 ADVANCE powder

diffractometer working in Bragg Brentano geometry with Cu-K $\alpha_{1,2}$ radiation and Lineal LinxEye detector. The diffractometer was operated over the angular range $2\theta = 10\text{--}70^\circ$ for qualitative analysis and $2\theta = 10\text{--}140^\circ$ for Rietveld analysis, using a step size of 0.015° in 2θ and acquisition time of 1 s per step. The data analysis was performed by the Rietveld method using the Jana program [22]. The background was interpolated between manually selected points. To model the peak profiles, a Cagliotti-type function with three parameters was used for the Gaussian part, and two parameters for the Lorentzian contribution. Additionally, an anisotropic broadening correction along $[001]$ was taken into account, probably related to a decrease of the coherent domain size in this direction. Atomic coordinates were refined as well as anisotropic atomic displacement parameters (ADPs) for heavy atoms (Y, Zr and Mn) and identical isotropic ADP for O atoms, with no oxygen sub- or over-stoichiometry, in agreement with Overton et al. [21]. The standard deviation values were corrected according to Berar and Lelann's description [23].

Each pure compound was mixed in equal amounts in weight with the most common 8YSZ electrolyte (8 mol%Y $_2$ O $_3$ zirconia, hereinafter abbreviated as 8YSZ; TZ-8Y, Tosoh Corporation), corresponding to stabilized cubic zirconia (S.G. *Fm-3m*). Then, the mixture was pressed into pellets and sintered at 1300°C for 8 h. Finally, the resulting powder was examined by XRD, as described above.

High-Temperature XRD (HT-XRD) was performed in air on a Rigaku Smartlab diffractometer equipped with an Anton Paar DHS1100 Heating device. The samples were placed in an alumina sample holder. Data were collected in the range $2\theta = 13\text{--}64^\circ$ (total counting time = 10 min per scan), with a 0.010° step, every 25°C from room temperature (RT) to 850°C . Cyclic Full Pattern Matching refinements were carried out with the FullProf software [24] and its graphical interface WinPLOTR [25]. The background was fitted with a 6-coefficient polynomial function. A pseudo-Voigt function was used to model profile shapes, including the Cagliotti function variables U , V , W , the Gaussian-Lorentzian mixing parameter η and two asymmetry parameters. The values of standard deviations were corrected according to Berar and Lelann's description [23].

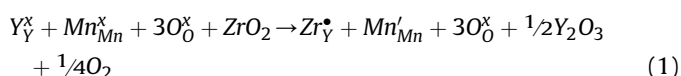
To probe the stability of the pure materials in reducing atmosphere, characteristic of the SOFC anode, ~ 0.3 g of each powder was heat treated at 800°C for 8 h in a tubular furnace fed with a wet H $_2$ /N $_2$ = 3/97 gas mixture ($Q = 5$ L h $^{-1}$ – pH $_2$ O ~ 0.03 atm), before being analysed by XRD. Considering those preliminary results, high-Temperature XRD (HT-XRD) was also carried in H $_2$ /N $_2$ = 3/97 without water bubbling (more reducing conditions) using a Bruker D8 diffractometer equipped with an Anton Paar XRK900 Reactive Chamber. The sample was placed in a Macor $^\circ$ glass-ceramic sample holder and the data were collected in the range $2\theta = 13\text{--}70^\circ$ (total counting time = 15 min per scan), with a 0.015° step in two segments: (i) from RT to 500°C every 50°C and (ii) from 500 to 800°C every 20°C before cooling (one scan every 100°C). The same heating and cooling rate of 0.1°C s^{-1} was used in all those measurements. The cell parameters were cyclically refined, applying the same procedure as for air data.

Thermogravimetric analysis in reducing atmosphere was carried out on 500 mg of each pure material by using a house-made high precision thermobalance (stability ± 10 μg at 1100°C for several days) as described in Ref. [26]. The experiment was carried out at fixed temperatures, in a H $_2$ /Ar = 2/98 reducing atmosphere, using a 100 mL min $^{-1}$ flow. An electrochemical system of oxygen pump gauge was coupled to the thermobalance, able to measure and control the oxygen partial pressure (pO $_2$) of the gas getting through the sample.

3. Results and discussion

3.1. Synthesis and structural characterization

The XRD patterns of Y $_{1-x}$ Zr $_x$ MnO $_3$ samples with $x = 0$ to 0.15 are shown in Fig. 2(a). For $x = 0$ and 0.05, the materials were found pure, considering the detection limit of the technique. On the contrary, the materials with $x > 0.10$, even after several heat treatments up to 1450°C , exhibited a hexagonal phase, apparently isostructural to YMnO $_3$ (S.G. *P6 $_3$ cm*), and an increasing amount of YSZ-type cubic phase. Indeed, a careful analysis of the $x = 0.10$ composition showed a very small peak characteristic of Y-doped zirconia at $2\theta = 34.9^\circ$, much more intense for higher Zr content (see Fig. 2(b)). These results are in disagreement with the description given by Van Aken et al. [14], which assert that it is possible to obtain pure donor-doped compounds for all compositions with contents $x < 0.30$ by using solid state synthesis at 1400°C . On the other hand, they confirms the results of Katsufuji et al. describing the solubility limit of Zr in YMnO $_3$ at $x \sim 0.1$ [15]. When comparing the diffraction patterns along with Zr doping, a peak shift towards higher angles is observed especially for $(00l)$ peaks whereas (hko) peaks such as (110) at $2\theta \sim 29^\circ$ remain almost unchanged (Fig. 2(c)). This suggests a cell contraction along c with a parameter nearly constant. Structural refinements using XRD data were performed using the Rietveld method for the samples corresponding with $x = 0$ to 0.10. As it can be seen in Fig. 2, some (hkl) peaks are especially broad, which can be interpreted as a particle size anisotropy; such phenomenon could be taken into account with one refined parameter for anisotropic broadening along $[001]$. Refinements results are reported in Table 1 and an example of graphical result for Rietveld refinement in the case of $x = 0.05$ is given in supplementary information section. The evolution of lattice parameters a and c , as well as cell volume V is represented in Fig. 3 as a function of Zr content. The first observations are confirmed, i.e. a parameter remains constant while c strongly drops when Zr is substituted for Y, leading to a cell volume contraction. Such behaviour is in agreement with the effective ionic radii values of Zr $^{4+}$ ($r_{\text{Zr}^{4+}} = 0.84$ and Y $^{3+}$ ($r_{\text{Y}^{3+}} = 1.019$ Å) for eightfold ($Z = 8$) coordination [27]. According to Van Aken et al. [14], the charge compensation for inserting Zr $^{4+}$ at the Y $^{3+}$ site leads to a change of Mn oxidation number from Mn $^{3+}$ to Mn $^{2+}$ according to the following reaction, using Kröger-Vink notation:



Despite the increase in mean Mn $^{2+/3+}$ ionic radius [27], the cell contraction would be explained by the progressive shift of all atoms towards a position of higher symmetry in the Zr-doped manganites. Such atomic displacements would straighten the MnO $_5$ bipyramids in Y $_{1-x}$ Zr $_x$ MnO $_3$, initially tilted with respect to the c -axis in YMnO $_3$ -phase, resulting also in non-buckled Y $^{3+}$ layers associated to the increase and (strong) decrease of the a and c cell parameters, respectively, and therefore of the drop in unit cell volume of Zr-doped compounds [8].

It is worth noting that the presence of the YSZ impurity for $x \geq 0.10$ is not indeed problematic for the application as SOFC electrode, because Y-doped zirconia is the commonly used SOFC electrolyte. This is especially true considering that most of the electrode materials that are effectively used in SOFC are generally not pure phases, but mixed with the same YSZ ionic conductor, either to enhance the thermal or chemical compatibility with the electrolyte, or to promote the ionic conductivity within the electrode.

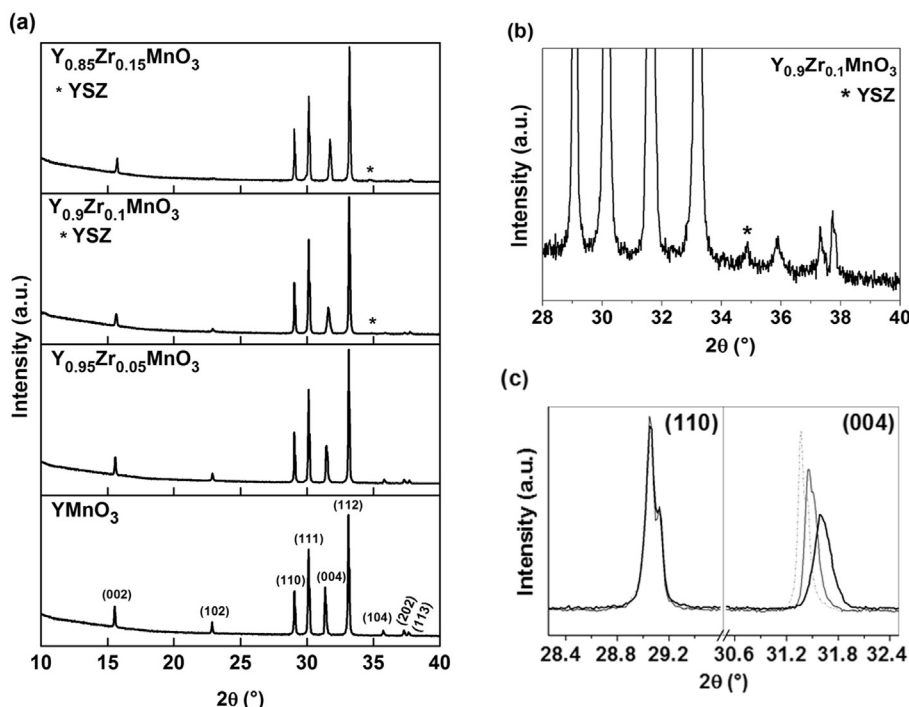


Fig. 2. X-Ray diffraction patterns of (a) $Y_{1-x}Zr_xMnO_3$ ($0 \leq x \leq 0.15$) (with hkl positions) (b) zoom of the $x = 0.10$ composition showing the weak amount of YSZ as impurity (c) (110) and (004) peaks evolution for $x = 0$ (black line), $x = 0.05$ (gray line) and $x = 0.1$ (dash-dot line).

Table 1

Structural parameters of $P6_3cm$ $Y_{1-x}Zr_xMnO_3$ ($x = 0, 0.05$ and 0.10) after synthesis, as obtained from Rietveld refinement using XRD data.

Sample	a (Å)	c (Å)	V (Å ³)	Reliability factors	
x = 0	6.1403 (3)	11.3952 (5)	372.08 (3)	R_p (%) = 2.37 wR_B (%) = 3.55	R_{wp} (%) = 3.20 χ^2 = 1.45
x = 0.05	6.1398 (3)	11.3619 (6)	370.93 (3)	R_p (%) = 3.12 wR_B (%) = 3.26	R_{wp} (%) = 4.35 χ^2 = 1.56
x = 0.10	6.1405 (4)	11.3171 (8)	369.55 (4)	R_p (%) = 3.16 wR_B (%) = 5.35	R_{wp} (%) = 4.49 χ^2 = 1.74

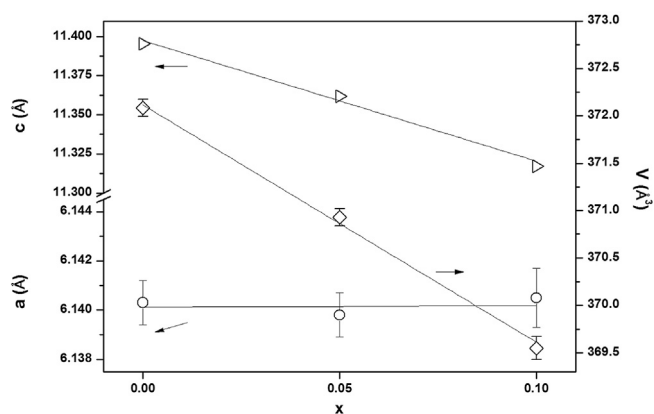


Fig. 3. Evolution as a function of x of cell parameters (\circ) a , (\triangleright) c and (\diamond) volume (V) in the $Y_{1-x}Zr_xMnO_3$ series.

3.2. High temperature reactivity with 8YSZ electrolyte

The XRD patterns of YZM/8YSZ mixtures ($x = 0$ to 0.10) corresponding to 50/50 wt ratio are depicted in Fig. 4, before and after heat treatment at 1300 °C in air. No detrimental reactivity between

both phases was observed, as no impurity phase was formed, even at such high temperature of reaction. This confirms, in the case of $YMnO_3$, the first result obtained by Huang *et al.* [18]. The diffraction peaks of the hexagonal phase are shifted to higher angles after reactivity test, *i.e.* the refined lattice parameters a and c , listed in Table 2, were considerably reduced in comparison to the original values ones. On the other hand, the YSZ lattice parameter increases after heat treatment. Such behaviour suggests a cross-diffusion phenomenon at the interface between the grains of YSZ and the $Y_{1-x}Zr_xMnO_3$, in which Y^{3+} cations, larger in size than Zr^{4+} ($r_{Y^{3+}} = 1.019$ Å and $r_{Zr^{4+}} = 0.84$ Å for $Z = 8$ coordination [27]), migrate to the electrolyte, while Zr^{4+} cations move toward the manganite, as schematized in Fig. 5. Such behaviour means an absence of risk for long-term degradation of the electrode-electrolyte interface because in case of reaching the limit of Zr in the manganite, the thermodynamic equilibrium at the YZM/YSZ interface would not involve any third phase (possibly insulating). It would not be detrimental to zirconia conductivity since XRD data suggest an increase in Y^{3+} concentration within the electrolyte material and not the contrary. In addition, the diffusion of $Mn^{2+/3+}$ cations ($r_{Mn^{3+}} = 0.58$ Å) into YSZ material, with possible mixed $Mn^{2+/3+}$ valence in the zirconia, cannot be ruled out, too, as some authors indicate that the solubility of Mn in 8YSZ varies between 5 mol% at 1000 °C and 15 mol% at 1500 °C [28]. Such doping of YSZ

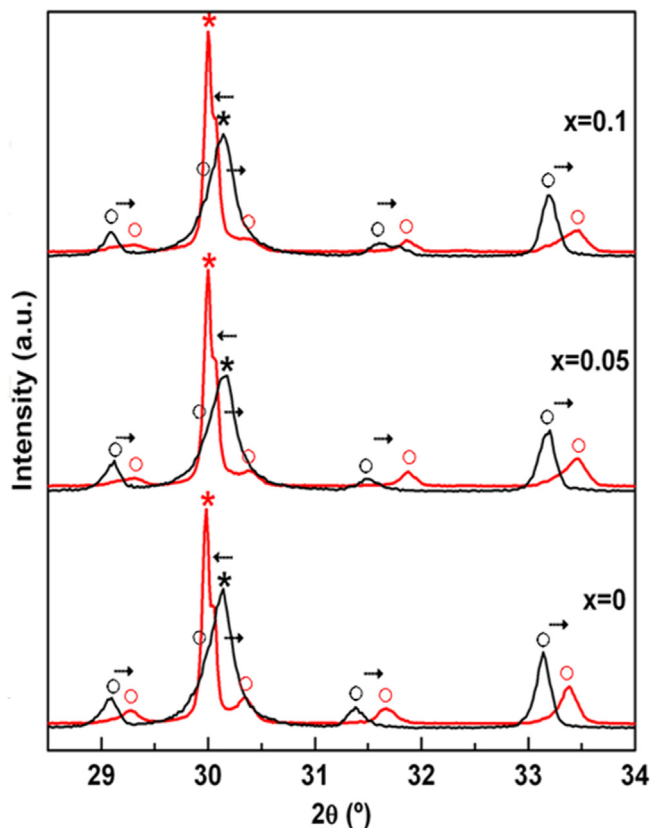


Fig. 4. XRD patterns of YZM/YSZ mixtures before (black) and after (red) chemical reactivity tests at 1300 °C for 8 h in air. In the figure, (○) and (*) symbols indicate YZM and YSZ phases, respectively. (For interpretation of the references to colour in this figure legend, the reader is referred to the web version of this article.)

Table 2

Structural parameters of mixtures $Y_{1-x}Zr_xMnO_3$ ($x = 0, 0.05$ and 0.10) with YSZ heat-treated at 1300 °C, as obtained from Rietveld refinement using XRD data.

Sample	a (Å)	c (Å)	V (Å ³)	Reliability factors
x = 0	6.0996 (3)	11.2955 (7)	363.95 (3)	$R_p(\%) = 2.85$ $R_{wp}(\%) = 3.79$
YSZ	5.1584 (1)	—	137.26 (2)	$\chi^2 = 1.22$
x = 0.05	6.0971 (8)	11.2279 (13)	361.48 (7)	$R_p(\%) = 3.28$ $R_{wp}(\%) = 4.28$
YSZ	5.1558 (2)	—	137.06 (4)	$\chi^2 = 1.45$
x = 0.10	6.1044 (8)	11.233 (2)	362.50 (9)	$R_p(\%) = 3.40$ $R_{wp}(\%) = 4.54$
YSZ	5.1545 (2)	—	136.95 (6)	$\chi^2 = 1.43$

with manganese has been shown to decrease the ionic conductivity, and increases the electronic conductivity of the material in the entire oxygen chemical potential range from 10^{-15} – 10^5 Pa, but with still high oxygen ion transport numbers (e.g. $t_{ion} = 0.99$ for Mn 4 mol% doped YSZ) [29]. Finally, the cross diffusion of Zr^{4+} and Y^{3+} at the YZM/YSZ interface can also be viewed as a benefit in terms of adhesion of the two layers, when sintering one over the other. The aforementioned behaviour constitutes a really interesting result, considering that the electrode-electrolyte reactivity has been for a long time considered as one of the majored issues to be solved in SOFC, in part solved in $(La,Sr)MnO_{3-\delta}$ using an A-site substoichiometry and/or limited sintering temperatures [5,19,30]. On the contrary, due to their yttrium and zirconium common elements, YZM and YSZ are able to coexist under the referred conditions and probably also in long-term conditions, which means that it would be possible to prepare YZM/YSZ composites in case of insufficient electrocatalytic activity of the manganite.

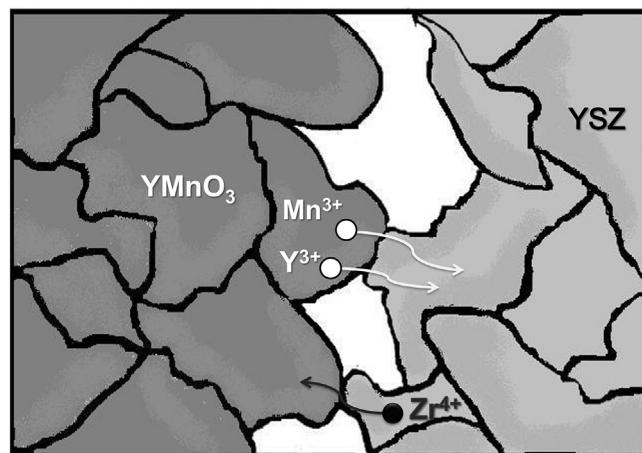


Fig. 5. Schematic representation of the crossed diffusion of Zr^{4+} , Y^{3+} and Mn^{3+} at the YZM/YSZ interface after reactivity test in air.

3.3. High temperature behaviour in air

Fig. 6 shows the *in situ* evolution in air of XRD pattern of $YMnO_3$ as a function of temperature. No particular feature can be observed in terms of structural change, i.e. the crystal structure remains the same corresponding to the polar $P6_3cm$ space group until 850 °C. Indeed, as recently described by Gibbs *et al.* [8], a structural transition to the centrosymmetric $P6_3/mmc$ space group occurs for $YMnO_3$ but at the higher temperature of 985 ± 14 °C. On the other hand, instead of general shift of all the diffraction peaks to lower angles, as expected for classical thermal expansion of the material, the thorough examination of XRD data shows once again an anisotropic behaviour with some peaks (and in particular all the (00l)) shifted to higher angles due to a contraction of c parameter. Cyclic Rietveld refinement of cell parameters using HT-XRD data confirms such behaviour, as shown by the evolution of a , c and cell volume V as a function of temperature (**Fig. 7**). An almost linear temperature dependence of the a -axis parameter is observed up to 850 °C without any noticeable slope change. At the same time, the c -axis parameter decreases, and the cell volume shows a similar

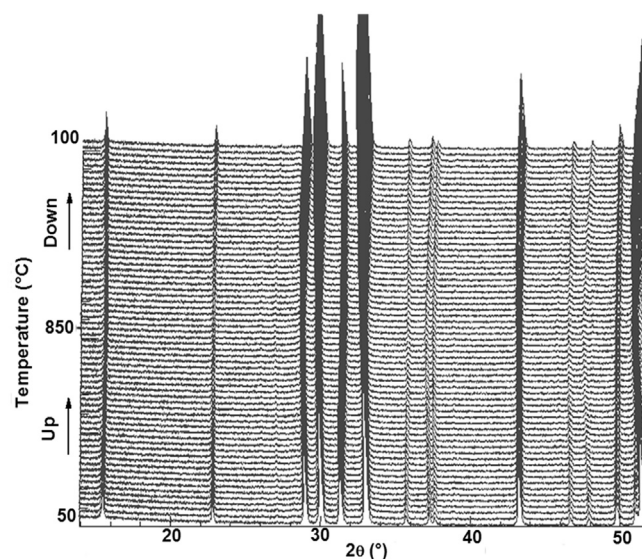


Fig. 6. HT-XRD patterns of $YMnO_3$ recorded in air from RT to 800 °C.

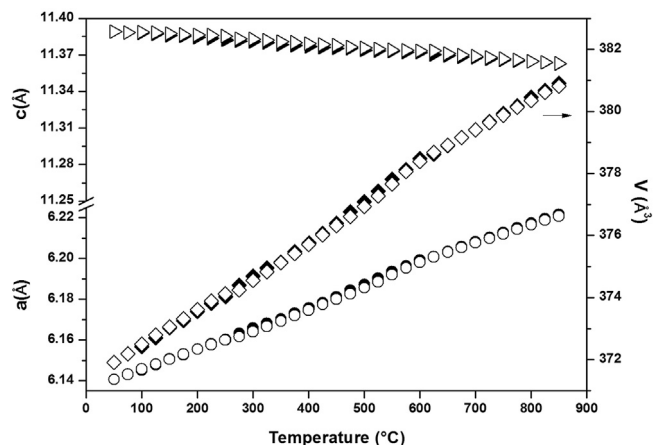


Fig. 7. Temperature dependence in air of (○) *a*, (▷) *c* and (◇) *V* parameters for YMnO₃.

trend to the *a*-axis parameter. Nevertheless, similarly to DyMnO₃, an unusual shift of lattice parameters occurs within the 300–600 °C range, that seems to be related to a change of oxygen content in the oxygenated compound in this range of temperature. Such feature is out of the scope of the present study but will be considered in a forthcoming work dealing with TGA and *in situ* ND experiments [20].

Even when considering this phenomenon, a good correspondence between heating and cooling curves is found and the nearly linear dependency of both cell parameters against *T* allows the determination of Thermal Expansion Coefficients (TEC) for both *a* and *c*-axis: $\alpha_a = 16.68 \times 10^{-6} \text{ K}^{-1}$ and $\alpha_c = -2.97 \times 10^{-6} \text{ K}^{-1}$. A volumetric expansion coefficient β can be calculated using the axial symmetry formula:

$$\beta = (2\alpha_a + \alpha_c) \quad (2)$$

It gives a value of $\beta = 30.39 \times 10^{-6} \text{ K}^{-1}$, which can be compared to the β value of $31\text{--}33 \times 10^{-6} \text{ K}^{-1}$ generally found for 8YSZ [31]. Such values are very close and, in a similar way as between YSZ and the La/Sr manganites ($\beta \sim 33\text{--}36 \times 10^{-6} \text{ K}^{-1}$ [5] and references therein), should normally not induce any thermal expansion mismatch between the electrode and electrolyte, which is the major cause of stress and failure at the interface between the two layers.

3.4. High temperature behaviour in reducing atmosphere

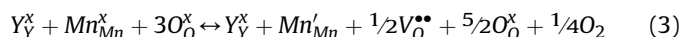
To probe the stability of the synthesized materials in reducing atmosphere, the materials were placed at 800 °C in wet reducing atmosphere characteristic of the SOFC anode compartment. The XRD diagrams of the as-obtained materials are plotted in Fig. 8. As it can be seen, all YZM family members are not stable in such conditions, regardless the presence of Zr or not at the Y site. Such results preclude their use as anode materials in Solid Oxide Fuel Cells. To study the possibility of using those materials at lower temperature, HT-XRD experiments on YMnO₃ sample were carried out in dry H₂/N₂ = 3/97 atm until 800 °C. The results are depicted in Fig. 9 (the same experiment was also carried out in wet reducing atmosphere until 500 °C without any significative change in the observed behaviour and refined cell parameters):

- (1) In dry reducing conditions, from RT to 500 °C, the yttrium manganite remains stable and no phase transition is

observed. Most of the diffraction peaks shift with temperature but with no obvious general trend of increase or decrease of all the cell parameters (anisotropic behaviour). Using cyclic structure refinement, the evolution of cell parameters can be plotted as a function of temperature, as depicted in Fig. 10. As in the previous case of thermal behaviour in air, *a* and *c*-axis parameters behaves differently: *a* value strongly increases from 6.1403 to 6.1964 Å corresponding to a $\Delta a/a = 1.3\%$ chemical expansion between RT and 500 °C, while the *c* value smoothly drops from 11.3952 to 11.3856 Å, i.e. a negative chemical expansion of $\Delta c/c = -0.00596\%$. A positive mean volumetric expansion of $\Delta V/V = 2.76\%$ was found. According to Fu et al. [30], such redox expansion would induce strong stresses on the adjacent components, especially on the electrolyte layer in an anode-supported cell or in large size cells, and would then be redhibitory. A solution to such issue would be the use of graded electrode YZM/YSZ, considering the good chemical compatibility between both materials described above.

- (2) Beyond 500 °C, a deviation from the linear behavior of the lattice parameters is observed. The increase of the slope change indicates a chemical contribution to the thermal expansion coefficient (TEC) which is related to the departure of oxygen from the sample. This oxygen loss is compensated by a partial reduction of Mn³⁺ into Mn²⁺. The higher ionic radii of Mn²⁺ compare to that of Mn³⁺ would explain the behaviour of lattice parameters with temperature. The structure finally decomposes around *T* ~700 °C, forming a mixture of MnO and Y₂O₃ oxides, what definitively precludes the use of YZM as SOFC anode material, a device for which a minimum temperature of 600 °C, and often higher than 700 °C, is generally considered. Different solutions are actually under study to try to stabilize the framework, including the substitution of Mn for other more stable cations, a strategy that has already proved to be efficient in the case of La/Sr chromo-manganite (LSCM), one of the best performing SOFC anode material [32–35].

In order to further examine the behaviour of YMnO₃ under reducing atmosphere conditions, thermogravimetric studies were carried out at fixed temperature (500 °C and 600 °C), varying the oxygen partial pressure (*p*O₂) using an electrochemical oxygen pump-gauge. According to literature, it can be assume YMnO₃ is nearly perfectly stoichiometric with full Mn³⁺ occupancy after synthesis in air [7,8,21]. As a consequence, a loss weight means the yttrium manganite becomes oxygen vacant due to Mn reduction, forming oxygen vacancies and resulting in a YMnO_{3-δ} stoichiometry, according to the following reaction:



The evolution of the oxygen content 3.δ as a function of log (*p*O₂) is given in Fig. 11. As it can be seen, YMnO_{3-δ} can withstand low oxygen partial pressure approaching *p*O₂ ~ 10⁻²⁹ atm without decomposing as the sample weight perfectly stabilizes in each point. This confirms the XRD results described previously. If the equilibrium constant of Eq. (3) is *K*(*T*), it can be easily demonstrated that:

$$K(T) = \left([V_O^{\bullet\bullet}] [Mn'_{Mn}]^2 p_{O_2}^{1/2} \right) / [O_O^x] \quad (4)$$

If $[V_O^{\bullet\bullet}]$ is small, it can be assumed that $[O_O^x] \sim 1$ and, according to (3), $2[V_O^{\bullet\bullet}] = [Mn'_{Mn}]$. It is obtained that:

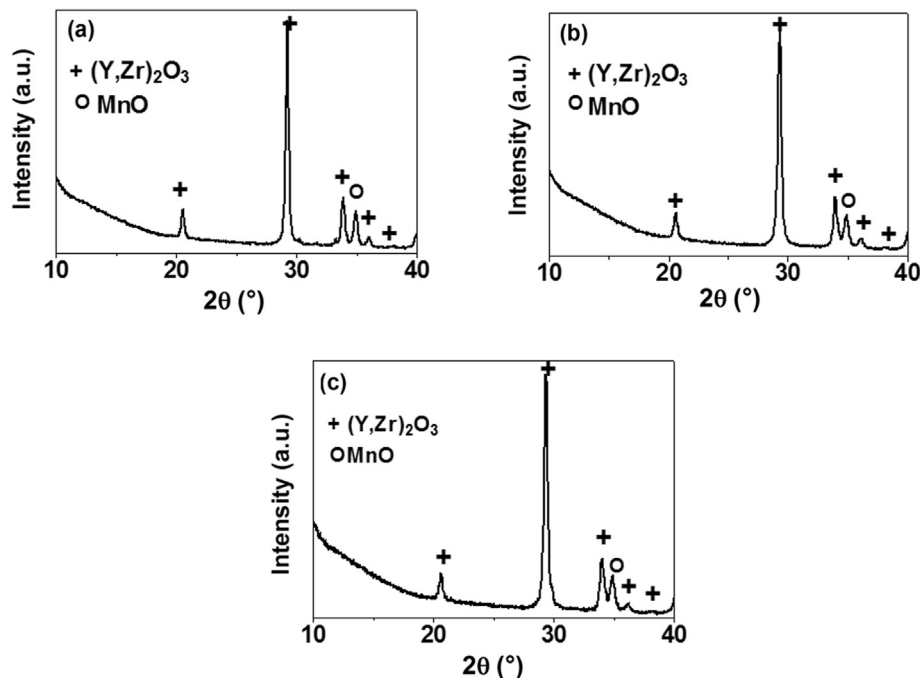


Fig. 8. XRD patterns of $Y_{1-x}Zr_xMnO_3$ ($0 \leq x \leq 0.10$) series after thermal treatment in wet diluted H_2 at 800 °C. (a) $YMnO_3$, (b) $Y_{0.95}Zr_{0.05}MnO_3$, (c) $Y_{0.9}Zr_{0.1}MnO_3$.

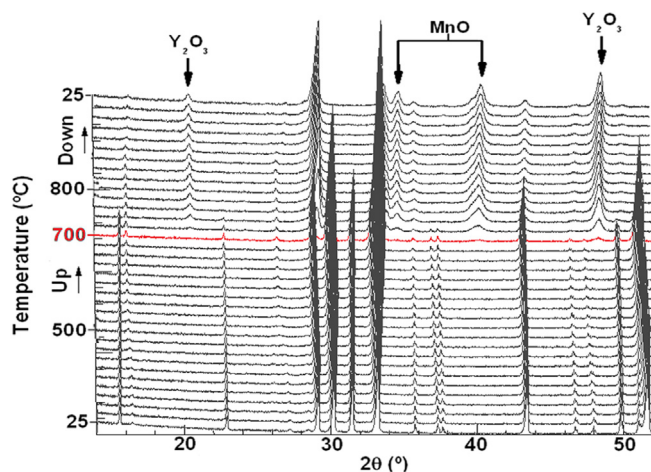


Fig. 9. HT-XRD patterns of $YMnO_3$ in dry $H_2/N_2 = 3/97$ reducing atmosphere.

$$K(T) = 4[V_O^{\bullet\bullet}]^3 pO_2^{1/2} \quad (5)$$

, which can be re-written:

$$\log[V_O^{\bullet\bullet}] = \log(\delta) = \frac{1}{3} \log K(T) - \frac{1}{3} \log 4 - \frac{1}{6} \log(pO_2) \quad (6)$$

, being δ the oxygen vacancies concentration. The inset in Fig. 11 represents the plot of $\log(\delta)$ as a function of $\log(pO_2)$, and gives a linear behaviour with a slope value of 0.155 very close to the theoretical 1/6 corresponding to Eq. (6). It confirms the hypothesis that the Mn^{3+} to Mn^{2+} reduction is compensated by the formation of double charged oxygen vacancies.

On the contrary, at 600 °C and in wet diluted hydrogen atmosphere ($pO_2 \sim 2.5 \times 10^{-23}$ atm; $pH_2/pH_2O \sim 1.4$), the sample weight cannot be stabilized, i.e. the material irreversibly decomposes into a

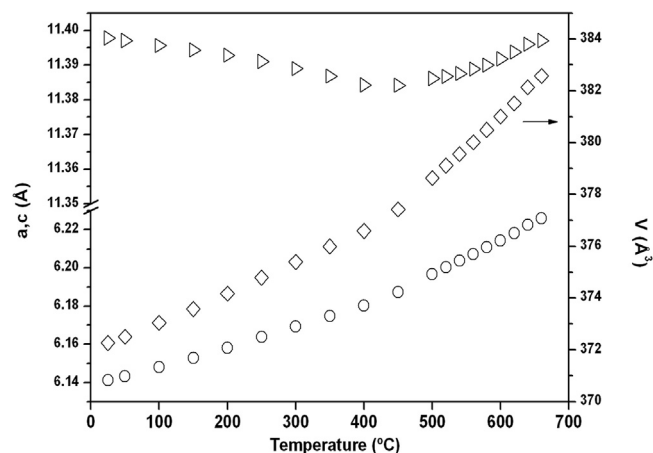


Fig. 10. Temperature dependence in dry $H_2/N_2 = 3/97$ of (○) a , (▷) c and (◇) V parameters for $YMnO_3$.

mixture Y_2O_3 and MnO , in quite fair agreement with XRD experiments, although the temperature of decomposition using the latter technique was found slightly higher (Fig. 9).

The same type of experiment has been carry out with $Y_{0.9}Zr_{0.1}MnO_{3-\delta}$ and the same behaviour was observed (not shown), i.e. a material stability at 500 °C in the range $0.25 < pH_2/pH_2O < 20.6$, remarkably similar to the undoped compound at the same temperature. It means that the stability of the material neither decreased nor improved with the addition of Zr dopant, probably because the substitution level is not sufficiently high and should better concern the Mn site.

4. Conclusions

The layered $Y_{1-x}Zr_xMnO_3$ compounds have been synthesized successfully up to Zr-contents of $x \approx 0.1$. The Zr-doping has a beneficial effect on the crystal structure as it decreases the $[MnO_5]$

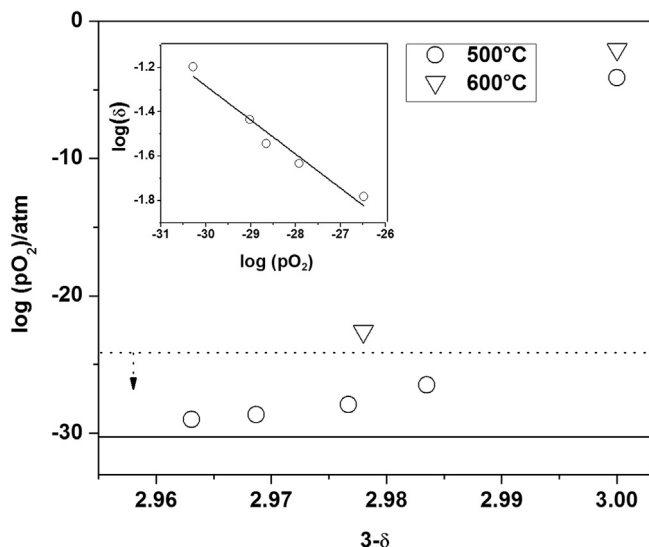


Fig. 11. Evolution of $\log(pO_2)$ vs. oxygen stoichiometry ($3-\delta$) for $YMnO_{3-\delta}$ at 500 °C (Δ) and 600 °C (\circ). In inset, plot of $\log(\delta)$ vs. $\log(pO_2)/\text{atm}$ at $T = 500$ °C, showing a $-1/6$ slope.

bi-pyramids tilting and corrugation of the Y^{3+} layers, what may be interesting for the application since it could be directly related to ionic conductivity as this is the case for many materials, e.g. for $La_{0.9}Sr_{0.1}Ga_{0.8}Mg_{0.2}O_{2.85}$ (LSGM) [34]. Unfortunately, undoped and Zr-doped $YMnO_3$ are unstable in reducing conditions beyond 600 °C, precluding their use as an SOFC anode component. Other doping elements at the Mn site are under study, with which we hope to stabilize the hexagonal layered structure type in hydrogen. Finally, this preliminary study shows that $Y_{1-x}Zr_xMnO_3$ compounds present interesting behaviour with respect to chemical reactivity and thermomechanical compatibility with YSZ electrolyte, revealing its potential for use as a cathode in the same devices.

Acknowledgments

We gratefully acknowledge the financial support of the *Vice-rectoría de Investigación y Extensión* of the *Universidad Industrial de Santander (UIS)* (Projects # 5465 and 1333). G.G. and Z.M. express their personal thanks to Dr. Mario Macías and M.Sc. Monica Sandoval from UIS for their useful advices, the *Laboratorio de Difracción de Rayos X (Parque Tecnológico Guatiguara-UIS)* for XRD measurements at RT. We also present our thanks to Dr. Liliana Mogni, Dr. Alejandra Montenegro, Dr. Jesús Vega and M.Sc. Diana Garcés for all the support at CNEA. The *Fonds Européen de Développement Régional (FEDER)*, *CNRS, Région Nord Pas-de-Calais* and *Ministère de l'Education Nationale de l'Enseignement Supérieur et de la Recherche* are also acknowledged for X-ray diffractometers' funding.

Appendix A. Supplementary data

Supplementary data related to this article can be found at <http://dx.doi.org/10.1016/j.jallcom.2016.08.125>.

References

- [1] S.C. Singhal, *Advances in solid oxide fuel cell technology*, *Solid State Ionics* 135 (2000) 305–313.
- [2] Y. Sun, J. Li, Y. Zeng, B.S. Amirkhiz, M. Wang, Y. Behnamian, J. Luo, A-site deficient perovskite: the parent for *in situ* exsolution of highly active, regenerable nanoparticles as SOFC anodes, *J. Mater. Chem. A* 3 (2015) 11048–11056.
- [3] EG&G Technical Services, Inc., *Fuel Cell Handbook*, seventh ed., US

- Department of Energy, Morgantown (West Virginia), 2004.
- [4] D. Rupasov, A. Chroneos, D. Parfitt, J.A. Kilner, R.W. Grimes, S. Ya, Istomin, Oxygen diffusion in $Sr_{0.75}Y_{0.25}CoO_{2.625}$: a molecular dynamics study, *Phys. Rev. B* 79 (2009) 172102.
- [5] K. Kendall, N.Q. Minh, S.C. Singhal, *High Temperature Solid Oxide Fuel Cells: Fundamentals, Design and Applications*, Elsevier, Oxford, 2003.
- [6] A. Atkinson, S. Barnett, R.J. Gorte, J.T.S. Irvine, A.J. McEvoy, M.B. Mogensen, S.C. Singhal, J. Vohs, Advanced anodes for high-temperature fuel cells, *Nat. Mater.* 3 (2004) 17–27.
- [7] B.B. Van Aken, A. Meetsma, T.T.M. Palstra, Hexagonal $YMnO_3$, *Acta Crystallogr. C* 57 (2001) 230–232.
- [8] A.S. Gibbs, K.S. Knight, P. Lightfoot, High-temperature phase transitions of hexagonal $YMnO_3$, *Phys. Rev. B* 9 (83) (2011) 094111.
- [9] H.L. Yakel, On the structures of some compounds of the perovskite type, *Acta Crystallogr.* 8 (1955) 394.
- [10] H.L. Yakel, W.C. Koehler, E.F. Bertaut, E.F. Forrat, On the crystal structure of the manganese(III) trioxides of the heavy lanthanides and yttrium, *Acta Crystallogr.* 16 (1963) 957.
- [11] H.W. Brinks, H. Fjellvåg, A. Kjekshus, Synthesis of metastable perovskite-type $YMnO_3$ and $HoMnO_3$, *J. Solid State Chem.* 129 (1997) 334–340.
- [12] A. Waintal, J. Chevanas, Transformation sous haute pression de la forme hexagonale de $Mn^{IV}O_3$ ($T = Ho, Er, Tm, Yb, Lu$) en une forme perovskite, *Mater. Res. Bull.* 2 (1967) 819–822.
- [13] P.A. Salvador, T.D. Doan, B. Mercey, B. Raveau, Stabilization of $YMnO_3$ in a perovskite structure as a thin film, *Chem. Mater.* 10 (1998) 2592–2595.
- [14] B.B. Van Aken, J.W.G. Bos, R.A. De Groot, T.T.M. Palstra, Asymmetry of electron and hole doping in $YMnO_3$, *Phys. Rev. B* 6312 (12) (2001) 125127.
- [15] T. Katsufuji, M. Masaki, A. Machida, M. Moritomo, K. Kato, E. Nishibori, M. Takata, K. Ohoyama, K. Kitazawa, H. Takagi, Crystal structure and magnetic properties of hexagonal $RMnO_3$ ($R = Y, Lu$, and Sc) and the effect of doping, *Phys. Rev. B* 13 (66) (2002) 1344341–1344348.
- [16] C. Moure, D. Gutiérrez, J.F. Fernández, J. Tartaj, P. Durán, O. Pena, Phase transitions induced on hexagonal manganites by the incorporation of aliovalent cations on A or B site, *Boletín de la sociedad española de Cerámica y Vidrio* 5 (38) (1999) 417–420.
- [17] D. Vega, G. Polla, A.G. Leyva, P. König, H. Lanza, A. Esteban, H. Aliaga, M.T. Causa, M. Tovar, B. Alascio, Structural phase diagram of $Ca_{1-x}Y_xMnO_3$: characterization of phases, *J. Solid State Chem.* 2 (156) (2001) 458–463.
- [18] T.-J. Huang, Y.-S. Huang, Electrical conductivity and YSZ reactivity of $Y_{1-x}Sr_xMnO_3$ as SOFC cathode material, *Mater. Sci. Eng. B-Solid* 103 (2003) 207–212.
- [19] T. Atsumi, T. Ohgushi, H. Namikata, N. Kamegashira, Oxygen nonstoichiometry of $LMnO_3$ ($LN = La, Pr, Nd, Sm$ and Y), *J. Alloy. Compd.* 252 (1997) 67–70.
- [20] S. Remsen, B. Dabrowski, O. Chmaissem, J. Mais, A. Szewczyk, Synthesis and oxygen content dependent properties of hexagonal $DyMnO_{3+\delta}$, *J. Solid State Chem.* 184 (2011) 2306–2314.
- [21] A.J. Overton, J.L. Best, I. Saratovsky, M.A. Hayward, Influence of topotactic reduction on the structure and magnetism of the multiferroic $YMnO_3$, *Chem. Mater.* 21 (2009) 4940–4948.
- [22] V. Petricek, M. Dusek, L. Palatinus, The Crystallographic Computing System, Institute of Physics, Praha, Czech Republic, 2006. <http://jana.fzu.cz/>.
- [23] J.F. Béar, P. Lelann, ESDs and estimated probable-error obtained in Rietveld refinements with local correlation, *J. Appl. Cryst.* 24 (1991) 1–5.
- [24] J. Rodríguez-Carvajal, Recent developments of the program FULLPROF, in: *Commission on powder diffraction (IUCr), Newsletter* 26 (2001) 12–19.
- [25] J. Rodríguez-Carvajal, T. Roisnel, in: *Seventh European Powder Diffraction Conference (EPDIC 7)*, 2000, pp. 118–123.
- [26] Doctoral thesis D. Tobia, E. Winkler, División de Resonancias magnéticas, Instituto Balseiro, Comisión Nacional de Energía Atómica & Universidad de Cuyo, 2011.
- [27] R.D. Shannon, Revised effective ionic radii and systematic studies of interatomic distances in halides and chalcogenides, *Acta Crystallogr. Section A* 5 (32) (1976) 751–767.
- [28] C.C. Appel, Zirconia stabilized by Y and Mn: a microstructural characterization, *Ionics* 5–6 (1) (1995) 406–413.
- [29] T. Kawada, N. Sakai, H. Yokokawa, M. Dokiya, Electrical properties of transition-metal-doped YSZ, *Solid State Ionics* 53–56 (1992) 418–425.
- [30] Q.X. Fu, F. Tietz, D. Stöver, $La_{0.45}Sr_{0.6}Ti_{1-x}Mn_xO_{3-\delta}$ perovskites as new anode materials for solid oxide fuel cells, *J. Electrochem. Soc.* 4 (153) (2006) D74–D83.
- [31] F. Tietz, G. Stochniol, A. Naoumidis, in: *Proceedings of the 5th European Conference on Advanced Materials and Processes and Applications (Euromat' 97)*, 2, 1997, p. 271.
- [32] S. Tao, J.T.S. Irvine, A redox-stable, efficient anode for solid-oxide fuel cells, *Nat. Mater.* 2 (2003) 320–323.
- [33] J.C. Ruiz-Morales, J. Canales-Vázquez, J. Peña-Martínez, D.M. Marrero-López, P. Nuñez, On the simultaneous use of $La_{0.75}Sr_{0.25}Cr_{0.5}Mn_{0.5}O_{3+\delta}$ as both anode and cathode material with improved microstructure in Solid Oxide Fuel Cells, *Electrochim. Acta* 52 (1) (2006) 278–284.
- [34] X. Yang, J.T.S. Irvine, $(La_{0.75}Sr_{0.25})_{0.95}Mn_{0.5}Cr_{0.5}O_3$ as the cathode of solid oxide electrolysis cells for high temperature hydrogen production from steam, *J. Mater. Chem.* 18 (2008) 2349.
- [35] M. Feng, J.B. Goodenough, A superior oxide-ion electrolyte, *Eur. J. Solid State Inorg. Chem.* 31 (1994) 663–672.